

Title	Highly Fluorinated Nanospace in Porous Organic Salts with High Water Stability/Capability and Proton Conductivity
Author(s)	Ami, Takahiro; Oka, Kouki; Kitajima, Showa et al.
Citation	Angewandte Chemie – International Edition. 2024, 63(37), p. e202407484
Version Type	VoR
URL	<a href="https://hdl.handle.net/11094/98123">https://hdl.handle.net/11094/98123</a>
rights	This article is licensed under a Creative Commons Attribution-NonCommercial 4.0 International License.
Note	

***Osaka University Knowledge Archive : OUKA***

<https://ir.library.osaka-u.ac.jp/>

Osaka University

# Highly Fluorinated Nanospace in Porous Organic Salts with High Water Stability/Capability and Proton Conductivity

Takahiro Ami, Kouki Oka,\* Showa Kitajima, and Norimitsu Tohnai\*

**Abstract:** Water in hydrophobic nanospaces shows specific dynamic properties different from bulk water. The investigation of these properties is important in various research fields, including materials science, chemistry, and biology. The elucidation of the correlation between properties of water and hydrophobic nanospaces requires nanospaces covered only with simple hydrophobic group (e.g., fluorine) without impurities such as metals. This work successfully fabricated all-organic diamondoid porous organic salts (*d*-POSs) with highly fluorinated nanospaces, wherein hydrophobic fluorine atoms are densely exposed on the void surfaces, by combining fluorine substituted triphenylmethylamine (TPMA) derivatives with tetrahedral tetrasulfonic acid. This *d*-POSs with a highly fluorinated nanospace significantly improved their water stability, retaining their crystal structure even when immersed in water over one week. Moreover, this highly hydrophobic and fluorinated nanospace adsorbs 160 mL(STP)/g of water vapor at  $P_e/P_0=0.90$ ; this is the first hydrophobic nanospace, which water molecules can enter, in an all-organic porous material. Furthermore, this highly fluorinated nanospace exhibits very high proton conductivity ( $1.34 \times 10^{-2}$  S/cm) at 90 °C and 95 % RH. POSs with tailorable nanospaces may significantly advance the elucidation of the properties of specific “water” in pure hydrophobic environments.

## Introduction

Structures and functions of porous materials composed of organic molecules can be precisely and easily controlled by appropriately designing their constituent molecules. These materials have been extensively investigated for various applications, such as gas separation and storage,<sup>[1]</sup> catalysts and reaction sites,<sup>[2]</sup> and proton conduction.<sup>[3]</sup> Among these organic-based porous materials, metal–organic frameworks (MOFs), which are fabricated by combining metal elements and organic linkers via coordination bonds,<sup>[4]</sup> and covalent organic frameworks (COFs), which are fabricated by linking organic molecules via covalent bonds,<sup>[5]</sup> are representative examples. In contrast, noncovalent organic frameworks (*n*COFs), which are constructed by the self-assembly of organic molecules via noncovalent bonds,<sup>[6]</sup> are usually soluble in highly polar solvents. Moreover, although *n*COFs are all-organic porous materials, they form thermodynamically stable and precise structures with high crystallinity.<sup>[7]</sup> Usually, noncovalent bonds are weaker than coordination and covalent bonds; therefore, *n*COFs are considered to have low structural stability. However, among the non-covalent bonds, the highly ionic and rigid hydrogen bonds between acids and bases such as sulfonic acids and amines, called “charge-assisted hydrogen bonding”, form significantly robust structures with high structural stability.<sup>[8]</sup>

Previously, we focused on the charge-assisted hydrogen bonding between sulfo and amino groups, and reported that aromatic sulfonic acids and bulky triphenylmethylamine (TPMA) hierarchically form robust diamondoid porous organic salts (*d*-POSs) via the formation of [4 + 4] supramolecular clusters (Figures 1a and 1b).<sup>[8c,9]</sup> *d*-POSs exhibit high thermal stability and structural robustness even after the removal of template molecules. However, the hydrogen bonds of most POSs are susceptible to attack by water molecules, and therefore *d*-POSs are usually unstable in the presence of water. Therefore, their crystal structures usually collapse or undergo phase transition under high humidity conditions or in water.<sup>[9a]</sup>

*d*-POSs exhibit various porous structures based on the molecular design of sulfonic acids and amines.<sup>[10]</sup> In particular, we demonstrated that introducing substituents at the *para*- and *meta*-positions of the phenyl rings of TPMA resulted in the exposure of these substituents on the void surfaces of the *d*-POSs, which significantly changed their void environments.<sup>[11]</sup>

This work aims to improve the water stability of *d*-POSs, and we focused on fluorine substituents with excellent water-repellency and hydrophobicity. To improve the hydro-

[\*] T. Ami, Prof. Dr. K. Oka, S. Kitajima, Prof. Dr. N. Tohnai  
 Department of Applied Chemistry,  
 Graduate School of Engineering, Osaka University,  
 2-1 Yamadaoka, Suita, Osaka 565-0871, Japan  
 E-mail: tohnai@chem.eng.osaka-u.ac.jp

Prof. Dr. K. Oka  
 Institute of Multidisciplinary Research for Advanced Materials,  
 Tohoku University,  
 2-1-1 Katahira, Aoba-ku, Sendai, Miyagi 980-8577, Japan  
 E-mail: oka@tohoku.ac.jp

© 2024 The Author(s). Angewandte Chemie International Edition published by Wiley-VCH GmbH. This is an open access article under the terms of the Creative Commons Attribution Non-Commercial License, which permits use, distribution and reproduction in any medium, provided the original work is properly cited and is not used for commercial purposes.

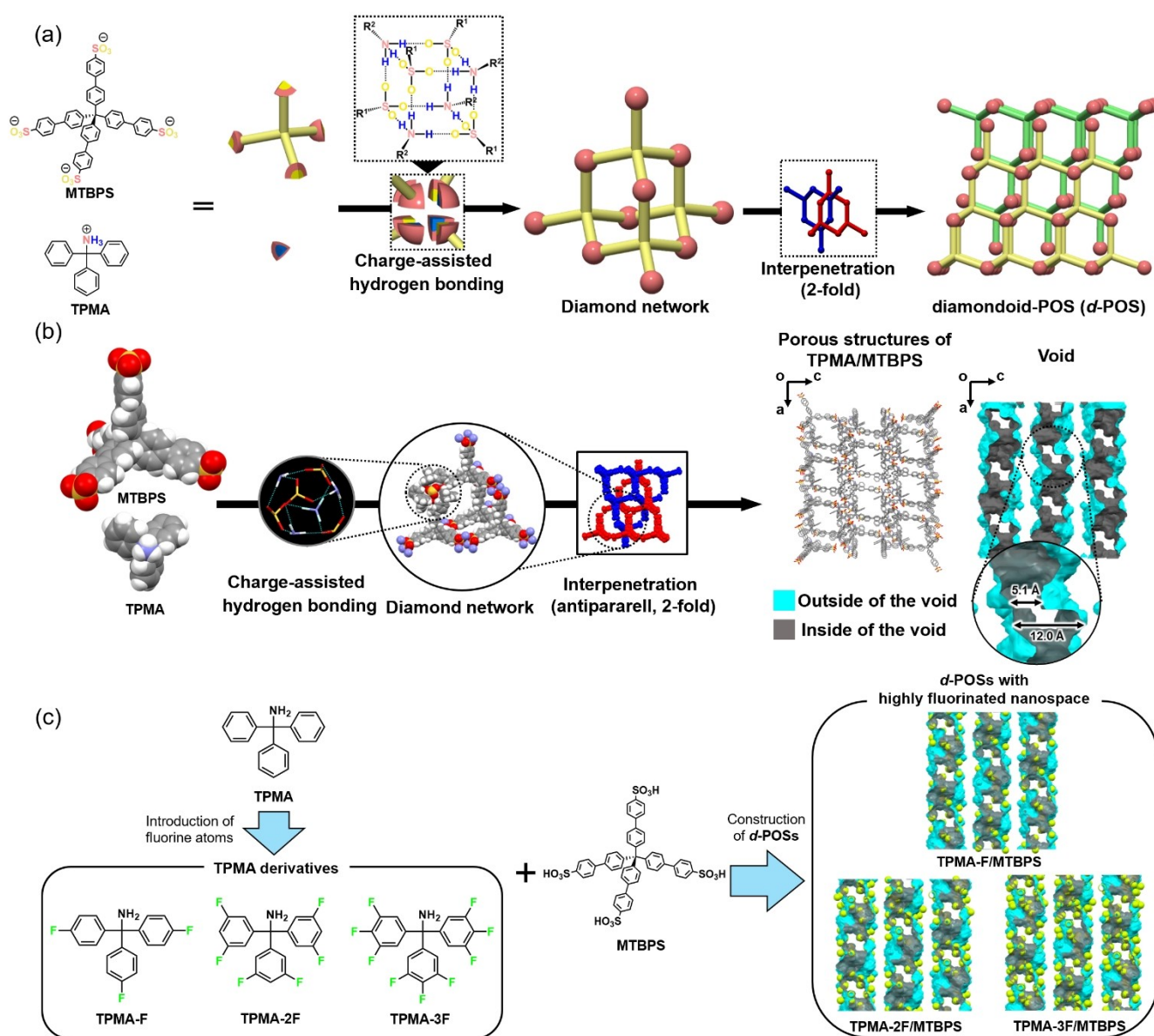


**Figure 1.** Formation of diamondoid porous organic salts (*d*-POSs) using tetrahedral-structured tetrasulfonic acid (MTBPS) and triphenylmeth-ylamine (TPMA). (a) Schematic of the formation of *d*-POS from MTBPS and TPMA via charge-assisted hydrogen bonding. (b) Schematic of the fabrication of *d*-POS using MTBPS and TPMA, and the resultant porous and void structures of TPMA/MTBPS. (c) Fabrication of *d*-POSs with highly fluorinated nanospaces using MTBPS and fluorine-substituted TPMA derivatives.

phobicity and water stability of frameworks of MOFs and COFs, the strategies such as introducing the hydrophobic group into an organic component,<sup>[12]</sup> coating the void surface with the hydrophobic polymer,<sup>[13]</sup> and combining with other hydrophobic material (e.g. fluorinated graphene oxide)<sup>[14]</sup> are aggressively investigated. Among them, introducing hydrophobic fluorine substituents has been most widely used for improving the hydrophobicity and water stability of frameworks.<sup>[15]</sup> In fact, in the fluorinated MOFs and COFs, the water stability improved with increasing the hydrophobicity of frameworks, and therefore this strategy is expected to be effective for improving the water stability of POSs. As shown in Figure 1c, TPMA derivatives are synthesized by introducing fluorine substituents at the *para*-

and *meta*-positions of the phenyl rings. These TPMA derivatives are combined with 4',4'',4''',4''''-methanetetrayltetrakis ([1,1'-biphenyl]-4-sulfonic acid) (MTBPS), which is a tetrahedral tetrasulfonic acid to fabricate *d*-POSs with highly fluorinated nanospaces in which fluorine atoms are densely exposed on the void surface. In addition, the density of fluorine in this highly fluorinated nanospace is the highest among all organic-based porous materials. As expected, the *d*-POS with a highly fluorinated nanospace exhibited significantly high water stability.

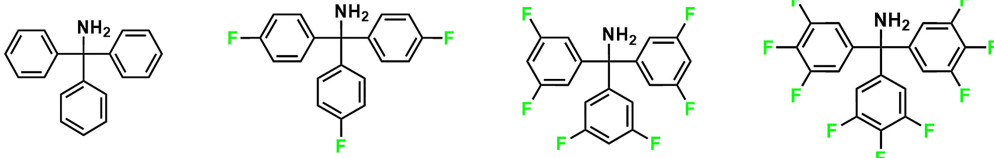
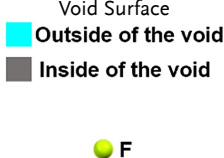
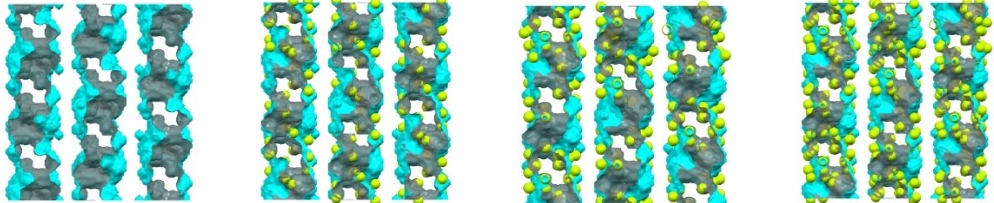
## Results and Discussion

As shown in Figure 1b, we previously reported that organic salts composed of TPMA and MTBPS, which have tetrahedral structures, resulted in the formation of *d*-POS (TPMA/MTBPS) via recrystallization with benzonitrile (a template molecule that facilitates the formation of porous structures) in a good solvent such as *N,N*-dimethylformamide (DMF),<sup>[11b,16]</sup> and TPMA/MTBPS exhibited high structural robustness. However, as shown in Figure S1, the hydrogen bonds in the crystal structure of TPMA/MTBPS are easily attacked by water molecules, and therefore TPMA/MTBPS is usually unstable in the presence of water molecules (that is, at high humidity conditions or in water). In contrast, the phenyl rings of TPMA were exposed on the void surfaces of the *d*-POSs, and introduced substituents into the phenyl rings of TPMA also exposed on their void surfaces. Therefore, the introduction of appropriate substituents can control their void environments.<sup>[11a]</sup> This work aimed to improve the water stability of *d*-POSs, and we focused on fluorine substituents with excellent water-repellency and hydrophobicity. As shown in Figure 1c, left, three types of TPMA derivatives, namely tris(4-fluorophenyl)methylamine (TPMA-F), tris(3,5-difluorophenyl)methylamine (TPMA-2F), and tris(3,4,5-trifluorophenyl)methylamine (TPMA-3F), were synthesized by introducing fluorine substituents into the *para*- and/or *meta*-positions of the phenyl rings of TPMA (the details of the synthesis procedure are written in Supporting Information). As shown in Figure 1c, right, these TPMA derivatives were then combined with MTBPS to fabricate *d*-POSs (TPMA-F/MTBPS, TPMA-2F/MTBPS, TPMA-3F/MTBPS), in which fluorine atoms are exposed on the void surfaces. In this work, the recrystallization conditions were reevaluated using benzonitrile as the template molecule and *N,N*-dimethylacetamide (DMA) as a good solvent. As shown in Figure S2, powder X-ray diffraction

(PXRD) data exhibited that the porous structure of TPMA-F/MTBPS in this work differed from that of TPMA-F/MTBPS in our previous report.<sup>[11a]</sup> On the other hand, the PXRD pattern of TPMA-F/MTBPS in this work coincided with that of TPMA/MTBPS, which have strong peaks at  $2\theta = 4.64, 5.58$  (Figure S3), and therefore this indicated the porous structure of TPMA-F/MTBPS in this work is identical to that of TPMA/MTBPS. In fact, the porous structure of TPMA-F/MTBPS, which was analyzed by single crystal X-ray structure analysis, exhibited almost the same crystal parameters as that of TPMA/MTBPS (Table S1). In addition, as shown in Figure S3, the porous structures of TPMA-2F/MTBPS and TPMA-3F/MTBPS were also identical to that of TPMA/MTBPS. Therefore, three porous structures identical to TPMA/MTBPS and with different amounts of substituted fluorine atoms were successfully constructed. The void environments of these fluorine-containing POSs were evaluated using structural simulations based on the crystal structure of TPMA/MTBPS (Table 1). As listed in Table 1, line 2, the number of fluorine atoms in these *d*-POSs increased with increasing amounts of substituted fluorine atoms of TPMA. The number of fluorine atoms per unit volume was  $3.1/1000 \text{ \AA}^3$  for TPMA-F/MTBPS,  $6.1/1000 \text{ \AA}^3$  for TPMA-2F/MTBPS, and  $9.2/1000 \text{ \AA}^3$  for TPMA-3F/MTBPS. Furthermore, as listed in Table 1, line 3, the porosity of these *d*-POSs slightly decreased with increasing amounts of substituted fluorine atoms, but their porous structures were identical to that of TPMA/MTBPS, and therefore these *d*-POSs maintained a high porosity of approximately 40%. In particular, although TPMA-3F/MTBPS had a high porosity of 38.4%, the substituted fluorine atoms were very densely exposed on its void surface, and therefore a highly fluorinated nanospace was successfully formed.

The porous structures of the *d*-POSs before and after the removal of the template molecules were analyzed by PXRD

**Table 1:** Environment of the void surfaces, number of substituted fluorine atoms per unit volume, exposure rate on the void surfaces of the fluorine atoms, and porosity of the *d*-POSs.

TPMA Derivatives				
	TPMA	TPMA-F	TPMA-2F	TPMA-3F
				
The number of F (per unit volume)	–	$3.1/1000 \text{ \AA}^3$	$6.1/1000 \text{ \AA}^3$	$9.2/1000 \text{ \AA}^3$
Porosity (PLATON)	40.7%	39.8%	39.2%	38.4%



(Figure S4). The crystallinity of TPMA/MTBPS without fluorine substituents significantly decreased after drying to remove the template molecules. Therefore, TPMA/MTBPS requires a time-consuming process, such as the supercritical fluid carbon dioxide (SCFCO<sub>2</sub>) process, for the removal of the template molecules.<sup>[11a]</sup> In contrast, as shown in Figures S4b and S4d, TPMA-F/MTBPS, TPMA-2F/MTBPS, and TPMA-3F/MTBPS enabled easy removal of the template molecules by drying at 25 or 70 °C, while maintaining a high crystallinity. This is presumably attributed to the weakened interactions between the void surfaces of the *d*-POSSs and the template molecules owing to the exposure of fluorine atoms on the void surfaces. For the *d*-POSSs before the removal of the template molecules, the structural transitions of the porous structures with increasing temperature and thermal stability were characterized by variable temperature-PXRD (VT-PXRD)<sup>[17]</sup> (Figure S5) and thermogravimetric analysis (TGA) (Figure S6) measurements, respectively. As shown in Figures S5–S7 and Table S2, the thermal stability of the *d*-POSSs with highly fluorinated nanospaces was improved by increasing the number of fluorine substituents. In particular, TPMA-3F/MTBPS exhibited the highest thermal stability among the *d*-POSSs, maintaining its porous structure without structural transition up to 265 °C, which is the decomposition point of the organic salts.

After the removal of the template molecules, as shown in Figure S8, the porosity of the *d*-POSSs with highly fluorinated nanospaces was evaluated by N<sub>2</sub> adsorption (−196 °C) and CO<sub>2</sub> adsorption (−78 °C) measurements. As listed in Table S3, the N<sub>2</sub>-Brunauer–Emmett–Teller (BET) surface areas calculated from the N<sub>2</sub> adsorption isotherms of TPMA-F/MTBPS, TPMA-2F/MTBPS, and TPMA-3F/MTBPS were 447 m<sup>2</sup>/g, 282 m<sup>2</sup>/g, and 410 m<sup>2</sup>/g, respectively. Furthermore, the CO<sub>2</sub>-BET surface areas calculated from the CO<sub>2</sub> adsorption isotherms of TPMA-F/MTBPS, TPMA-2F/MTBPS, and TPMA-3F/MTBPS were 481 m<sup>2</sup>/g, 325 m<sup>2</sup>/g, and 678 m<sup>2</sup>/g, respectively. These results indicate that the introduction of fluorine substitution significantly influenced the void environments of the *d*-POSSs and increased their N<sub>2</sub>- and CO<sub>2</sub>-BET surface areas (for further details regarding the gas adsorption measurements, please see the gas adsorption section in the Supporting Information).

In the presence of water, ascribed to attacking hydrogen bonds from the water molecules, which enter the void space of *d*-POSSs, the unsubstituted TPMA/MTBPS was unstable. As shown in Figure 2a, the crystallinity of TPMA/MTBPS completely disappeared after 1 day under conditions of 25 °C and 100 % RH. This is a very common characteristic of *d*-POSSs. *d*-POSSs with high water stability have not yet been reported. However, the developed *d*-POSSs possess exposed fluorine atoms with excellent water-repellency on the void surface. Therefore, it is considered that water molecules are less likely to approach the hydrogen-bonded clusters and attack the hydrogen bonds in the *d*-POSSs. Therefore, the *d*-POSSs with highly fluorinated nanospaces were also exposed to 25 °C and 100 % RH for 1 day. As shown in Figure 2, the water stability of the *d*-POSSs was dramatically improved with an increase in the number of fluorine substituents. TPMA-3F/MTBPS, which has the highest fluorine density

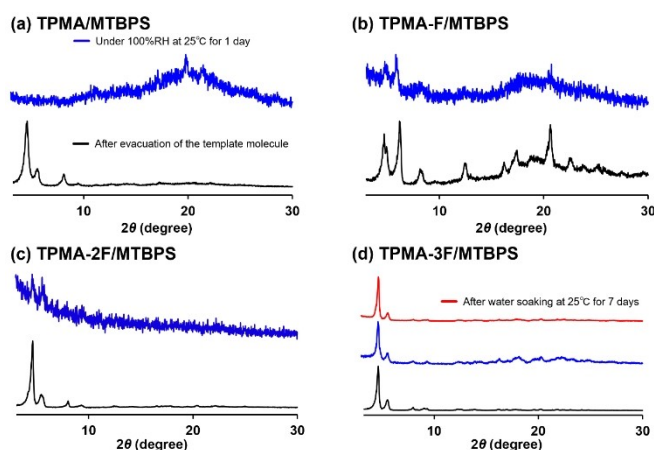


**Figure 2.** PXRD patterns of the POSSs. (a) TPMA/MTBPS, (b) TPMA-F/MTBPS, (c) TPMA-2F/MTBPS, and (d) TPMA-3F/MTBPS, after template removal (black), under 100 % RH at 25 °C for 1 day (blue), and after water immersion at 25 °C for 7 days (red).

on the void surface, maintained a high crystallinity even after 1 day under conditions of 25 °C and 100 % RH, demonstrating its high water stability even under high humidity conditions. Moreover, as shown in Figure 2d, TPMA-3F/MTBPS maintained its porous structure and high crystallinity even after being completely immersed in water for more than one week, and exhibited identical adsorption isotherm as before (Figure S9). Based on the above, the extremely high water stability of TPMA-3F/MTBPS was demonstrated.

To determine whether water molecules can enter the highly fluorinated nanospaces in TPMA-3F/MTBPS which has high water stability, water vapor adsorption measurements were performed at 25 °C. As shown in Figure 3, TPMA-3F/MTBPS adsorbed 160 mL(STP)/g of water vapor at  $P/P_0 = 0.90$ , indicating that water molecules can enter the highly fluorinated nanospaces, which is presumably attributed to its relatively large void size ( $> 10$  Å) as shown in Figure 1b. Therefore, although the void surface of this highly fluorinated nanospace is extremely water-repellent, it contains areas where water molecules can exist. Furthermore, by introducing hydrophobic fluorine atoms, TPMA-3F/MTBPS did not adsorb the water vapor at low pressure and drastically adsorbed at relatively high pressure ( $P/P_0 > 0.6$ ). The reference [18] reported that the introduction of fluorine substituents improves the hydrophobicity of the framework and strongly increases the activation energy barrier of the system for the diffusion of water. In addition, the other reference<sup>[19]</sup> reported that void surfaces adsorbed the water molecules in order of their hydrophilicity, and therefore as the hydrophobicity of the surface increased, a higher pressure for the adsorption of water molecules was required. In other words, the larger the percentage of hydrophobic surfaces in the entire void surface, the lower the amount of adsorption for water vapor at low pressure, and the higher the hydrophobicity of the void surface, the higher the pressure threshold for a rapid increase in water vapor adsorption. Furthermore, Figure 3 shows that TPMA-3F/

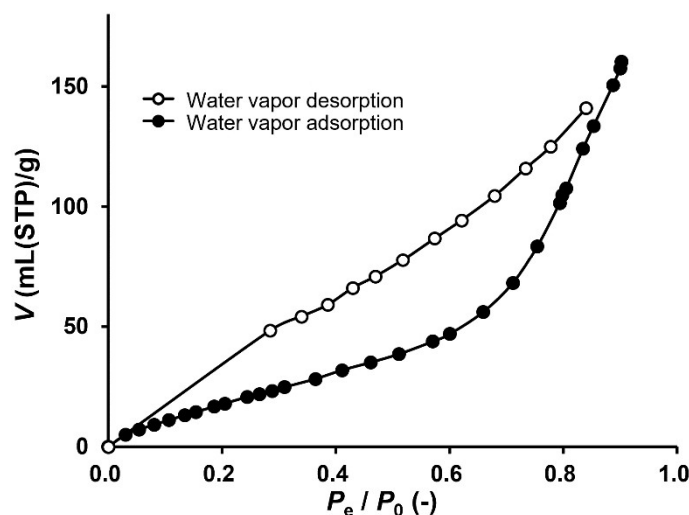


**Figure 3.** Water vapor adsorption/desorption isotherms of TPMA-3F/MTBPS ( $\text{H}_2\text{O}$ ,  $25^\circ\text{C}$ ).  $P_e$  represents the gas adsorption pressure and  $P_0$  represents the condensation pressure of the adsorbate at the measurement temperature. The maximum adsorption capacity of 160 mL(STP)/g at  $P_e/P_0=0.90$  in the water vapor absorption isotherm was converted to 7.14 mmol of water in 1 g of *d*-POS, and we calculated the number of units composed of a sulfonic acid molecule and four amine molecules, included in 1 g of *d*-POS. Then, the number of water molecules was divided by the number of a unit in 1 g of *d*-POS, and the relative water molecules absorbed/*d*-POS components were estimated.

MTBPS adsorbed 18.8 water molecules per MTBPS molecule and four TPMA-3F molecules. Although the void surface of TPMA-3F/MTBPS was covered with hydrophobic fluorine atoms, the highly fluorinated nanospace allowed numerous water molecules to exist at  $P_e/P_0=0.90$ . Moreover, as shown in Figure S10, TPMA-3F/MTBPS maintained a high crystallinity after the water vapor adsorption measurements, demonstrating its high stability for water molecules, which entered the void. On the other hand, other reported POSs materials are unstable in aqueous environments, and their structures are expected to collapse during water vapor adsorption measurements. Therefore, the accurate water adsorption capacities of other reported POSs materials have not been reported, and TPMA-3F/MTBPS is the first POS that is stable in water and exhibits water vapor adsorption. As listed in Table S4, the number of fluorine atoms per unit volume of TPMA-3F/MTBPS was extremely high among organic-based porous structures, in which water molecules can enter their voids and whose detailed structures have been reported. This indicates that the highly fluorinated nanospace in TPMA-3F/MTBPS is the most water-repellent and hydrophobic organic-based porous structure, which water molecules can enter.

Because of the extremely weak interactions with the void surface, water molecules reportedly form unique networks in hydrophobic nanospaces of MOFs (<3 nm to 4 nm), resulting in rapid water transport and high proton conductivity.<sup>[20]</sup> As shown in Figure 1b, right, the highly fluorinated nanospace in TPMA-3F/MTBPS has a maximum void size of approximately 1.2 nm (12 Å), and therefore, the water molecules in TPMA-3F/MTBPS are assumed to conduct protons. Therefore, the proton conductivity of pelletized TPMA-3F/MTBPS was measured by electrochemical impedance spectroscopy (EIS), as shown in Figures 4

and S11. Proton conductivity was calculated by fitting analysis, which assumed the equivalent circuit in Figure S12. Proton conduction in TPMA-3F/MTBPS did not show the typical dielectric relaxation under low humidity ( $25^\circ\text{C}$  and 30 % RH), and therefore TPMA-3F/MTBPS did not exhibit proton conductivity. In contrast, as shown in Figure 4b and Tables S5 and S6 under a high humidity condition ( $25^\circ\text{C}$  and 95 % RH), proton conduction in TPMA-3F/MTBPS exhibited dielectric relaxation, as indicated by the flattened semicircles corresponding to the bulk and grain boundary resistances in the high frequency range, and TPMA-3F/MTBPS had a proton conductivity of  $1.11 \times 10^{-5}$  S/cm. As shown in Table S7, the direct current (DC) electrical conductivity of  $9.59 \times 10^{-7}$  S/cm calculated by DC resistance measurements was smaller than  $1.11 \times 10^{-5}$  S/cm, indicating that TPMA-3F/MTBPS exhibits proton conductivity under high humidity conditions. Furthermore, under extremely high humidity conditions (95 % RH), the temperature dependence of proton conductivity for TPMA-3F/MTBPS was evaluated at various temperatures (Figure S11 and Tables S5 and S6). As shown in Figure 4b and Table S5, the proton conductivity of TPMA-3F/MTBPS increased with increasing temperature from  $2.18 \times 10^{-5}$  S/cm at  $30^\circ\text{C}$  to  $3.67 \times 10^{-4}$  S/cm at  $60^\circ\text{C}$ . Moreover, as shown in Table S8, TPMA-3F/MTBPS exhibited a high proton conductivity of  $1.34 \times 10^{-2}$  S/cm at  $90^\circ\text{C}$ , which is comparable to that of general Nafion ( $10^{-2}$  S/cm<sup>[21]</sup>) and higher than those of other organic-based porous materials, without the need for proton donors such as acids. In general, the proton conductivity improves with increasing temperature, and therefore proton-conductive materials are desirable to be used as high a temperature as possible.<sup>[22]</sup> However, the glass transition temperature of general Nafion is about  $120^\circ\text{C}$ .<sup>[21]</sup> Furthermore, when using Nafion at above  $140^\circ\text{C}$ , irreversible degradation is caused,

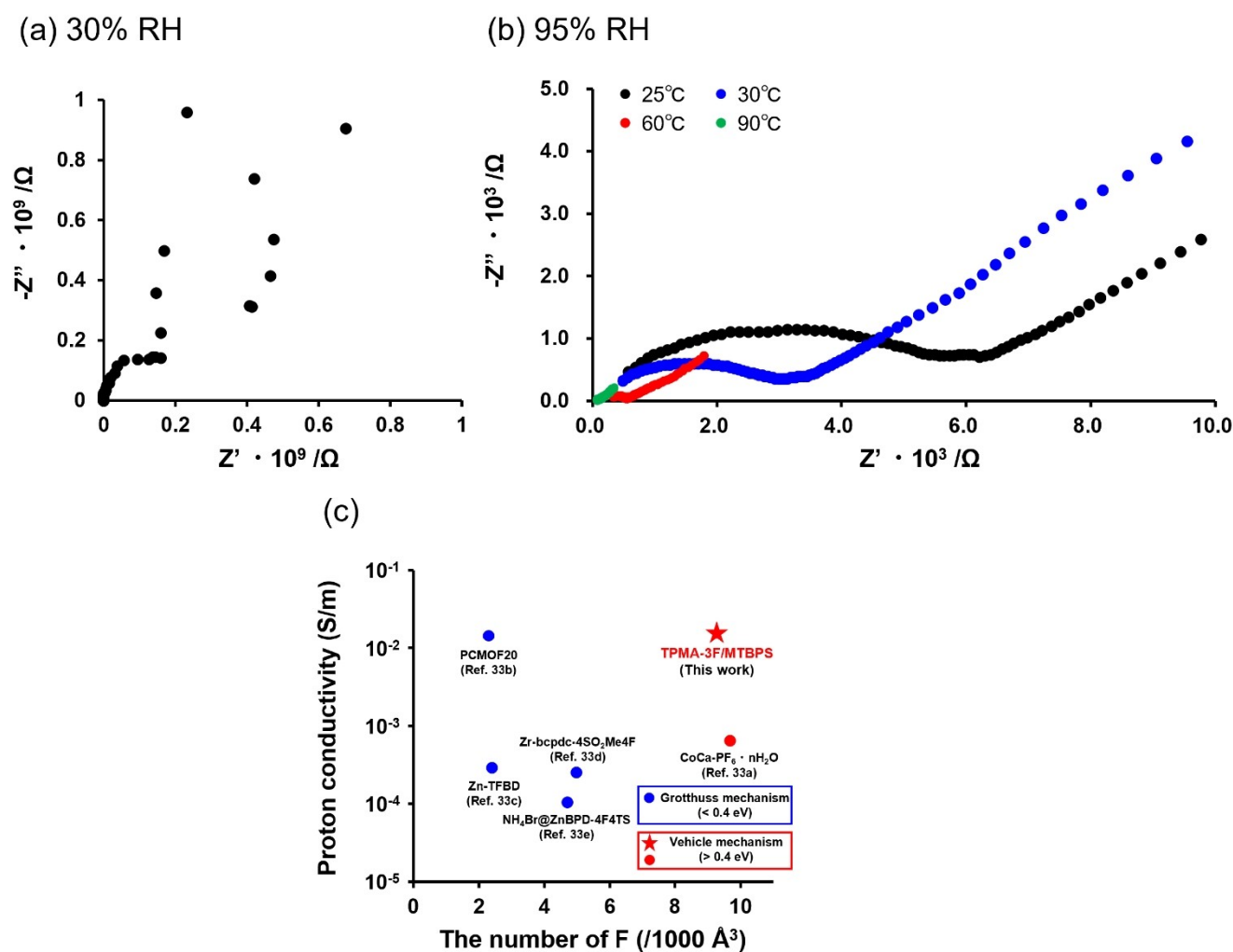


**Figure 4.** Proton conductivity of TPMA-3F/MTBPS. Impedance spectra of the disk-shaped pellets of TPMA-3F/MTBPS (a) under 30% RH and (b) under 95% RH at 25 °C (black), 30 °C (blue), 60 °C (red), and 90 °C (green). The flattened semicircles in the high-frequency region contain two components: bulk resistance and grain boundary resistance.<sup>[32]</sup> (c) The number of included fluorine atoms per unit volume and calculated proton conductivities at 90 °C comparison for TPMA-3F/MTBPS and previously reported porous structures with fluorinated nanospace.<sup>[33]</sup>

and its proton conductivity drastically decreases.<sup>[23]</sup> On the other hand, TPMA-3F/MTBPS have higher thermal stability (256 °C) compared to the general Nafion, and therefore TPMA-3F/MTBPS can be used at higher temperatures for improving the proton conductivity of the electrolyte membrane, and TPMA-3F/MTBPS can be facily regenerated by re-dissolving and recrystallization even in the case of a decrease in the crystallinity. In addition, as shown in Table S9, the crystal of TPMA-3F/MTBPS exhibited low density ascribed to its higher porosity of approximately 40 % than those of other proton-conducting POSs (< 20 %). Therefore, TPMA-3F/MTBPS is the lightest among the previously reported proton-conducting POSs with a high proton conductivity ( $> 10^{-2}$  S/cm),<sup>[24]</sup> and can help to further reduce the weight of the electrolyte membrane and expand applications of fuel cells using them.<sup>[25]</sup> Furthermore, as shown in Figure 4c and Table S10, TPMA-3F/MTBPS exhibited both a vast number of included fluorine atoms per unit volume and the extremely high proton conductivity

among porous structures with fluorinated nanospace. In the porous crystal of TPMA-3F/MTBPS, ascribed to all sulfo groups of MTBPS forming hydrogen bonds with the amino groups, sulfo groups of MTBPS cannot provide protons to the highly fluorinated nanospace. Therefore, in the case of proton conduction of TPMA-3F/MTBPS, the confined water is more likely to be the proton source. The confinement effect of the nanospace for water molecules greatly lowers the free energy barrier for self-dissociation, and enhances the self-dissociation process of water molecules.<sup>[26]</sup> As a result, confined water is reported to self-dissociate more readily, and exhibits an ionic product ( $K_w$ ) about two orders of magnitude greater than bulk water.<sup>[26]</sup> For example, the references<sup>[27]</sup> exhibited that the  $pK_a$  value of the confined water reached 6–7, and this acidity was comparable to that of the proton source in the hydrophobic nanospace with a diameter of 10 Å in the MOF, which exhibited the proton conductivity of  $10^{-2}$  S/cm.<sup>[20,28]</sup> Therefore, also in the hydrophobic nanospace with the similar diameters of 5.0–12 Å in

TPMA-3F/MTBPS, the self-dissociation of water presumably behaves as an excellent proton source. The reference<sup>[29]</sup> reported that the nanospace with a narrow bottleneck limited the hydration structure of hydroxide ions, and the vehicular diffusion of hydroxide ions was two orders of magnitude smaller than that of protons.<sup>[20]</sup> Therefore, the effects of hydroxide ions on the proton conduction in TPMA-3F/MTBPS were much smaller than the effects of protons, and hydroxide ions hardly influenced the proton conductivity.<sup>[30]</sup> In addition, fluorine atoms introduced on the surface of the nanospace have been reported to decrease the free energy of hydronium ions, and to stabilize them.<sup>[31]</sup> Therefore, the highly fluorinated nanospace in TPMA-3F/MTBPS should stabilize hydronium ions, and indirectly contribute to the increase in hydronium ions. Furthermore, free sulfo groups at the terminus of TPMA-3F/MTBPS may supply some protons. In the PXRD and NMR data of TPMA-3F/MTBPS after impedance measurement, although peak intensity decreased from before impedance measurement, the peak position was unchanged, and therefore the porous structure was maintained (Figures S14 and S15). Proton conduction in hydrophobic nanospaces under high humidity conditions using highly crystalline organic-based porous materials has only been observed in a few MOFs.<sup>[20]</sup> The observation of proton conduction in the hydrophobic nanospaces of all-organic porous materials has not been reported thus far. This is the first work to demonstrate proton conduction using a hydrophobic nanospace in an all-organic porous material.

Elucidating the proton conduction mechanism is crucial for analyzing and improving proton conductivity. Proton conduction is considered to occur via one of two mechanisms: the vehicle mechanism or the grothuss mechanism. In general, the rate-limiting step in the grothuss mechanism is considered to be the cleavage of hydrogen bonds.<sup>[34]</sup> Typical hydrogen bond energies are reported in the range from 0.1 to 0.4 eV,<sup>[35]</sup> and therefore the activation energy of the grothuss mechanism also ranges from 0.1 to 0.4 eV. In other words, at activation energies above 0.4 eV, proton conduction follows the vehicle mechanism, and at activation energies below 0.4 eV, it follows the grothuss mechanism. In the hydrophobic nanospaces of MOFs, water molecules form specific clusters, and protons are conducted through the hydrogen-bonded network between the clusters. Therefore, proton conduction in MOFs has been reported to follow the grothuss mechanism.<sup>[20]</sup> In this work, as shown in Figure S16, Arrhenius plots of the proton conductivity at each temperature under a high humidity condition (95 % RH) were used to estimate the activation energy ( $E_a$ ) for proton conduction in TPMA-3F/MTBPS. The  $E_a$  of proton conduction in TPMA-3F/MTBPS was 1.01 eV, indicating that proton conduction in TPMA-3F/MTBPS should follow the vehicle mechanism. This is ascribed to the fact that the hydrophobic fluorine atoms exposed on the void surface restrict the formation of hydrogen bonds between water molecules. G. He et al. reported on the dynamics of water molecules and hydronium ions in carbon nanotubes with different diameters (6.8–14 Å).<sup>[31a]</sup> In particular, this simulation calculated detailed relations between

the hydrophobicity of the surfaces, and the hydrogen bonding network or the abundance ratio of water molecules and hydronium ions in these carbon nanotubes, by gradually fluorinating the surfaces. This simulation revealed that as the hydrophobicity of the surface increases by fluorination, the dynamics of water molecules and hydronium ions are limited, and therefore the probability of forming hydrogen bonding between water molecules and hydronium ions decreases, regardless of the size of the diameter. The formation of hydrogen bonding is known to inhibit the self-diffusion of water molecules,<sup>[36]</sup> and therefore the improvement of the hydrophobicity of the surface by fluorination is considered to support the self-diffusion of hydronium ions following the vehicle mechanism. In addition, this simulation exhibited that fluorination of the surface of carbon nanotubes increases the number of hydronium ions and decreases the number of water molecules inside the carbon nanotubes. This indicated that the confinement effect of these fluorinated nanospace for water molecules greatly lowers the free energy barrier for self-dissociation and enhances the self-dissociation process of water molecules. Therefore, even in the highly fluorinated nanospace with the similar diameters of 5.0–12 Å in TPMA-3F/MTBPS, the self-dissociations of water molecules in the nanospace supply the protons, and these protons were most likely transferred as hydronium ions following the vehicle mechanism rather than via the specific hydrogen-bonded network of water molecules, were supported by past theoretical calculation.<sup>[31a,36]</sup> Furthermore, as shown in Figure 4c, only proton conductions in TPMA-3F/MTBPS and CoCa-PF<sub>6</sub>·nH<sub>2</sub>O,<sup>[33a]</sup> which include a vast number of fluorine atoms ( $>9/1000 \text{ Å}^3$ ), exhibited the high  $E_a$  ( $>0.5 \text{ eV}$ ), and proton conductions in other perfluoro spaces, which include a few number of fluorine atoms ( $<5/1000 \text{ Å}^3$ ), exhibited the low  $E_a$  ( $<0.4 \text{ eV}$ ). This is ascribed to the improvement of hydrophobicity of the void surfaces with increasing the density of fluorine, and consistent with the previous report<sup>[31a]</sup> that the highly hydrophobic pore surface restricts the continuous hydrogen bonding network of water molecules. Therefore, the vehicle mechanism presumably dominates proton conduction in highly hydrophobic nanospace, such as in TPMA-3F/MTBPS. From the above, the improvement of the number of included fluorine atoms per unit volume increases the  $E_a$  of proton conduction, and therefore the temperature dependence of proton conductivity becomes larger. In summary, this work revealed the excellent proton conductivity ( $1.34 \times 10^{-2} \text{ S/cm}$  at  $90^\circ\text{C}$ ) (Table S8) of the highly fluorinated nanospace in an all-organic porous material with highly hydrophobic nanospace for the first time.

## Conclusion

In this work, MTBPS, which has a tetrahedral structure, and TPMA derivatives with fluorine substituents at the *para*- and *meta*-positions of the phenyl rings were combined to fabricate *d*-POSSs with highly fluorinated nanospaces. For TPMA-3F/MTBPS, the highly fluorinated nanospace contained 9.2 fluorine atoms per  $1000 \text{ Å}^3$ , and these fluorine



atoms were densely exposed on the void surface. Ascribed to the water-repellent and hydrophobic fluorine atoms covering the void surface, this *d*-POS exhibited very high water stability and maintained its crystal structure even after immersion in water for more than one week. Furthermore, TPMA-3F/MTBPS adsorbed 160 mL(STP)/g of water vapor at  $P_0/P_0=0.90$ , which was attributed to its large porosity (38.4 %). This is the first report on water molecules entering hydrophobic nanospaces in an all-organic porous material. Moreover, the developed highly fluorinated hydrophobic nanospace promotes proton conduction, without the addition of proton donors such as acids, and water molecules in this highly fluorinated hydrophobic nanospace exhibit a high proton conductivity of  $1.34 \times 10^{-2}$  S/cm at 90 °C and 95 % RH. Furthermore, these extremely hydrophobic nanospaces without exposed metal elements on the void surface implied that proton conduction follows the vehicle mechanism, which differs from the complex hydrophobic nanospaces in previously reported porous materials.<sup>[20,33]</sup> This work also demonstrated that *d*-POSs are applied in aqueous environments. POSs with tailorable hydrophobic nanospaces may significantly advance the elucidation of the dynamic properties of specific “water” in pure hydrophobic environments.

## Acknowledgements

This work was partially supported by Grants-in-Aids for Scientific Research (No. JP20H02548, JP20H02714, JP22K14732, JP23H03827, and JP23K17945) from MEXT, Japan. K.O. also acknowledges the support from Amano Industry Technology Laboratory, Kenjiro Takayanagi Foundation, Masuyakinen basic research foundation, Shorai Foundation for Science and Technology, Sugiyama Houkoku-kai, TEPCO Memorial Foundation, and Yamada Science Foundation. T.A. acknowledges the support from JST SPRING, Grant number JPMJSP2138.

## Conflict of Interest

The authors declare no conflict of interest.

## Data Availability Statement

The data that support the findings of this study are available from the corresponding author upon reasonable request.

**Keywords:** porous organic salts • hydrophobic nanospace • highly fluorinated nanospace • water stability • proton conduction

- [1] a) P. Sozzani, S. Bracco, A. Comotti, L. Ferretti, R. Simonutti, *Angew. Chem. Int. Ed.* **2005**, *117*, 1850–1854. DOI: 10.1002/anie.200461704; b) M. L. Foo, R. Matsuda, Y. Hijikata, R. Krishna, H. Sato, S. Horike, A. Hori, J. Duan, Y. Sato, Y. Kubota, M. Takata, S. Kitagawa, *J. Am. Chem. Soc.* **2016**, *138*,

- 3022–3030. DOI: 10.1021/jacs.5b10491; c) J. Jiang, H. Furukawa, Y. B. Zhang, O. M. Yaghi, *J. Am. Chem. Soc.* **2016**, *138*, 10244–10251. DOI: 10.1021/jacs.6b05261; d) D. B. Gutierrez, E. B. Caldona, R. D. Espiritu, R. C. Advincula, *MRS Commun.* **2021**, *11*, 391–401. DOI: 10.1557/s43579-021-00062-8.
- [2] a) J. Baek, B. Rungtaweeworanit, X. Pei, M. Park, S. C. Fakra, Y. S. Liu, R. Matheu, S. A. Alshimri, S. Alshehri, C. A. Trickett, G. A. Somorjai, O. M. Yaghi, *J. Am. Chem. Soc.* **2018**, *140*, 18208–18216. DOI: 10.1021/jacs.8b11525; b) J. S. Lee, E. A. Kapustin, X. Pei, S. Llopis, O. M. Yaghi, F. D. Toste, *Chem* **2020**, *6*, 142–152. DOI: 10.1016/j.chempr.2019.10.022; c) K. Dey, S. Mohata, R. Banerjee, *ACS Nano* **2021**, *15*, 12723–12740. DOI: 10.1021/acsnano.1c05194.
- [3] a) Z.-C. Guo, Z.-Q. Shi, X.-Y. Wang, Z.-F. Li, G. Li, *Coord. Chem. Rev.* **2020**, *422*, 213465. DOI: 10.1016/j.ccr.2020.213465; b) D.-W. Lim, H. Kitagawa, *Chem. Soc. Rev.* **2021**, *50*, 6349–6368. DOI: 10.1039/D1CS00004G.
- [4] a) O. M. Yaghi, M. O’Keeffe, N. W. Ockwig, H. K. Chae, M. Eddaoudi, J. Kim, *Nature* **2003**, *423*, 705–714. DOI: 10.1038/nature01650; b) H. Furukawa, K. E. Cordova, M. O’Keeffe, O. M. Yaghi, *Science* **2013**, *341*, 1230444. DOI: 10.1126/science.1230444; c) J. K. Zareba, M. Nyk, M. Samoc, *Cryst. Growth Des.* **2016**, *16*, 6419–6425. DOI: 10.1021/acs.cgd.6b01090; d) Z. Ji, H. Wang, S. Canossa, S. Wuttke, O. M. Yaghi, *Adv. Funct. Mater.* **2020**, *30*, 2000238. DOI: 10.1002/adfm.202000238.
- [5] a) A. P. Cote, A. I. Benin, N. W. Ockwig, M. O’Keeffe, A. J. Matzger, O. M. Yaghi, *Science* **2005**, *310*, 1166–1170. DOI: 10.1126/science.1120411; b) C. S. Diercks, O. M. Yaghi, *Science* **2017**, *355*, eaal1585. DOI: 10.1126/science.aal1585; c) K. Geng, T. He, R. Liu, S. Dalapati, K. T. Tan, Z. Li, S. Tao, Y. Gong, Q. Jiang, D. Jiang, *Chem. Rev.* **2020**, *120*, 8814–8933. DOI: 10.1021/acs.chemrev.9b00550; d) K. Oka, B. Winther-Jensen, H. Nishide, *Adv. Energy Mater.* **2021**, *11*, 2003724. DOI: 10.1002/aenm.202003724.
- [6] R. B. Lin, Y. He, P. Li, H. Wang, W. Zhou, B. Chen, *Chem. Soc. Rev.* **2019**, *48*, 1362–1389. DOI: 10.1039/c8cs00155c.
- [7] J. Luo, J.-W. Wang, J.-H. Zhang, S. Lai, D.-C. Zhong, *CrystEngComm* **2018**, *20*, 5884–5898. DOI: 10.1039/c8ce00655e.
- [8] a) V. A. Russell, M. C. Etter, M. D. Ward, *J. Am. Chem. Soc.* **1994**, *116*, 1941–1952. DOI: 10.1021/ja00084a039; b) V. A. Russell, C. C. Evans, W. Li, M. D. Ward, *Science* **1997**, *276*, 575–579. DOI: 10.1126/science.276.5312.575; c) A. Yamamoto, S. Uehara, T. Hamada, M. Miyata, I. Hisaki, N. Tohnai, *Cryst. Growth Des.* **2012**, *12*, 4600–4606. DOI: 10.1021/cg300796u.
- [9] a) A. Yamamoto, T. Hamada, I. Hisaki, M. Miyata, N. Tohnai, *Angew. Chem. Int. Ed.* **2013**, *52*, 1709–1712. DOI: 10.1002/anie.201208153; b) A. Yamamoto, T. Hasegawa, T. Hamada, T. Hirukawa, I. Hisaki, M. Miyata, N. Tohnai, *Chem. Eur. J.* **2013**, *19*, 3006–3016. DOI: 10.1002/chem.201202959.
- [10] a) A. Yamamoto, T. Hirukawa, I. Hisaki, M. Miyata, N. Tohnai, *Tetrahedron Lett.* **2013**, *54*, 1268–1273. DOI: 10.1016/j.tetlet.2012.12.086; b) T. Miyano, N. Okada, R. Nishida, A. Yamamoto, I. Hisaki, N. Tohnai, *Chem. Eur. J.* **2016**, *22*, 15430–15436. DOI: 10.1002/chem.201602233.
- [11] a) T. Ami, K. Oka, K. Tsuchiya, N. Tohnai, *Angew. Chem. Int. Ed.* **2022**, *134*, e20222597. DOI: 10.1002/anie.202202597; b) T. Ami, K. Oka, K. Tsuchiya, W. Kosaka, H. Miyasaka, N. Tohnai, *CrystEngComm* **2023**, *25*, 2321–2325. DOI: 10.1039/D3CE00086A.
- [12] Q. Sun, H. He, W.-Y. Gao, B. Aguila, L. Wojtas, Z. Dai, J. Li, Y.-S. Chen, F.-S. Xiao, S. Ma, *Nat. Commun.* **2016**, *7*, 13300. DOI: 10.1038/ncomms13300.
- [13] W. Zhang, Y. Hu, J. Ge, H.-L. Jiang, S.-H. Yu, *J. Am. Chem. Soc.* **2014**, *136*, 16978–16981. DOI: 10.1021/ja509960n.

- [14] K. Jayaramulu, F. Geyer, M. Petr, R. Zboril, D. Vollmer, R. A. Fischer, *Adv. Mater.* **2017**, *29*, 1605307. DOI: 10.1002/adma.201605307.
- [15] a) W. B. Li, Y. Z. Cheng, D. H. Yang, Y. W. Liu, B. H. Han, *Macromol. Rapid Commun.* **2023**, *44*, 2200778. DOI: 10.1002/marc.202200778; b) S.-i. Noro, T. Nakamura, *NPG Asia Mater.* **2017**, *9*, e433–e433. DOI: 10.1038/am.2017.165; c) S. Kumar, B. Mohan, C. Fu, V. Gupta, P. Ren, *Coord. Chem. Rev.* **2023**, *476*, 214876. DOI: 10.1016/j.ccr.2022.214876.
- [16] Deposition Numbers 2152672 (TPMA/MTBPS) and 2333544 (TPMA-F/MTBPS) contain the supplementary crystallographic data for this paper. These data are provided free of charge by the joint Cambridge Crystallographic Data Centre and Fachinformationszentrum Karlsruhe Access Structures service [www.ccdc.cam.ac.uk/structures](http://www.ccdc.cam.ac.uk/structures).
- [17] A. E. Aliev, S. P. Smart, I. J. Shannon, K. D. Harris, *J. Chem. Soc. Faraday Trans.* **1996**, *92*, 2179–2185. DOI: 10.1039/FT9969202179.
- [18] A. H. Farmahini, D. S. Sholl, S. K. Bhatia, *J. Am. Chem. Soc.* **2015**, *137*, 5969–5979. DOI: 10.1021/jacs.5b01105.
- [19] A. Metrane, A. Delhali, M. Ouikhalfan, A. H. Assen, Y. Belmabkhout, *J. Chem. Eng. Data* **2022**, *67*, 1617–1653. DOI: 10.1021/acs.jced.2c00145.
- [20] K.-i. Otake, K. Otsubo, T. Komatsu, S. Dekura, J. M. Taylor, R. Ikeda, K. Sugimoto, A. Fujiwara, C.-P. Chou, A. W. Sakti, *Nat. Commun.* **2020**, *11*, 843. DOI: 10.1038/s41467-020-14627-z.
- [21] H.-Y. Jung, J. W. Kim, *Int. J. Hydrogen Energy* **2012**, *37*, 12580–12585. DOI: 10.1016/j.ijhydene.2012.05.121.
- [22] D. Langevin, Q. T. Nguyen, S. p Marais, S. m Karademir, J.-Y. Sanchez, C. Iojoiu, M. Martinez, R. g Mercier, P. Judeinstein, C. Chappey, *J. Phys. Chem. C* **2013**, *117*, 15552–15561. DOI: 10.1021/jp312575m.
- [23] a) J. T. Hinatsu, M. Mizuhata, H. Takenaka, *J. Electrochem. Soc.* **1994**, *141*, 1493. DOI: 10.1149/1.2054951; b) G. Alberti, M. Casciola, L. Massinelli, B. Bauer, *J. Membr. Sci.* **2001**, *185*, 73–81. DOI: 10.1016/S0376-7388(00)00635-9; c) F. Bauer, S. Denner, M. Willert-Porada, *J. Polym. Sci. Part B* **2005**, *43*, 786–795. DOI: 10.1002/polb.20367.
- [24] a) G. Xing, T. Yan, S. Das, T. Ben, S. Qiu, *Angew. Chem. Int. Ed.* **2018**, *57*, 5345–5349. DOI: 10.1002/anie.201800423; b) A. Karmakar, R. Illathvalappil, B. Anothumakkool, A. Sen, P. Samanta, A. V. Desai, S. Kurungot, S. K. Ghosh, *Angew. Chem. Int. Ed.* **2016**, *55*, 10667–10671. DOI: 10.1002/anie.201604534; c) M.-J. Wei, Y. Gao, K. Li, B. Li, J.-Q. Fu, H.-Y. Zang, K.-Z. Shao, Z.-M. Su, *CrystEngComm* **2019**, *21*, 4996–5001. DOI: 10.1039/C9CE00762H; d) Y. Wang, M. Zhang, Q. Yang, J. Yin, D. Liu, Y. Shang, Z. Kang, R. Wang, D. Sun, J. Jiang, *Chem. Commun.* **2020**, *56*, 15529–15532. DOI: 10.1039/D0CC05402J.
- [25] J. Yang, J. Wang, B. Hou, X. Huang, T. Wang, Y. Bao, H. Hao, *Chem. Eng. J.* **2020**, *399*, 125873. DOI: 10.1016/j.cej.2020.125873.
- [26] D. Munoz-Santiburcio, D. Marx, *Phys. Rev. Lett.* **2017**, *119*, 056002. DOI: 10.1103/PhysRevLett.119.056002.
- [27] a) A. Mandal, D. Guha, R. Das, S. Mitra, S. Mukherjee, *J. Chem. Phys.* **2001**, *114*, 1336–1343. DOI: 10.1063/1.1329641; b) M. Mukhopadhyay, A. Mandal, R. Misra, D. Banerjee, S. P. Bhattacharyya, S. Mukherjee, *J. Phys. Chem. B* **2009**, *113*, 567–573. DOI: 10.1021/jp804103h.
- [28] X.-x. Wang, H. Fu, D.-m. Du, Z.-y. Zhou, A.-g. Zhang, C.-f. Su, K.-s. Ma, *Chem. Phys. Lett.* **2008**, *460*, 339–342. DOI: 10.1016/j.cplett.2008.05.074.
- [29] D. Dong, W. Zhang, A. C. Van Duin, D. Bedrov, *J. Phys. Chem. Lett.* **2018**, *9*, 825–829. DOI: 10.1021/acs.jpclett.8b00004.
- [30] J. M. Bockris, A. K. Reddy, M. Gamboa-Aldeco, *Modern electrochemistry, Vol. 1*, Plenum Press, New York **1970**.
- [31] a) N. Zhang, Y. Song, X. Ruan, X. Yan, Z. Liu, Z. Shen, X. Wu, G. He, *Phys. Chem. Chem. Phys.* **2016**, *18*, 24198–24209. DOI: 10.1039/C6CP03012B; b) B. F. Habenicht, S. J. Paddison, M. E. Tuckerman, *J. Mater. Chem.* **2010**, *20*, 6342–6351. DOI: 10.1039/C0JM00253D.
- [32] N. E. Wong, P. Ramaswamy, A. S. Lee, B. S. Gelfand, K. J. Bladck, J. M. Taylor, D. M. Spasyuk, G. K. Shimizu, *J. Am. Chem. Soc.* **2017**, *139*, 14676–14683. DOI: 10.1021/jacs.7b07987.
- [33] a) S. S. Bao, Y. X. Wu, N. Z. Li, L. M. Zheng, *Eur. J. Inorg. Chem.* **2016**, *2016*, 4476–4482. DOI: 10.1002/ejic.201600203; b) Z. Hassanzadeh Fard, N. E. Wong, C. D. Malliakas, P. Ramaswamy, J. M. Taylor, K. Otsubo, G. K. Shimizu, *Chem. Mater.* **2018**, *30*, 314–318. DOI: 10.1021/acs.chemmater.7b04467; c) L. Hou, X. Jing, H. Huang, C. Duan, *Chem. Commun.* **2023**, *59*, 3407–3410. DOI: 10.1039/D3CC00257H; d) W.-R. Xian, Y. He, Y. Diao, Y.-L. Wong, H.-Q. Zhou, S.-L. Zheng, W.-M. Liao, Z. Xu, J. He, *Inorg. Chem.* **2020**, *59*, 7097–7102. DOI: 10.1021/acs.inorgchem.0c00576; e) H.-Q. Zhou, S.-L. Zheng, C.-M. Wu, X.-H. Ye, W.-M. Liao, J. He, *Molecules* **2021**, *26*, 5044. DOI: 10.3390/molecules26165044.
- [34] a) X. Meng, H.-N. Wang, S.-Y. Song, H.-J. Zhang, *Chem. Soc. Rev.* **2017**, *46*, 464–480. DOI: 10.1039/C6CS00528D; b) P. Ramaswamy, N. E. Wong, G. K. Shimizu, *Chem. Soc. Rev.* **2014**, *43*, 5913–5932. DOI: 10.1039/C4CS00093E; c) N. Agmon, *Chem. Phys. Lett.* **1995**, *244*, 456–462. DOI: 10.1016/0009-2614(95)00905-J.
- [35] M. A. Lantz, S. P. Jarvis, H. Tokumoto, T. Martynski, T. Kusumi, C. Nakamura, J. Miyake, *Chem. Phys. Lett.* **1999**, *315*, 61–68. DOI: 10.1016/S0009-2614(99)01201-4.
- [36] N. Zhang, W. Li, C. Chen, J. Zuo, L. Weng, *Mol. Phys.* **2013**, *111*, 939–949. DOI: 10.1080/00268976.2012.760050.

Manuscript received: April 19, 2024

Accepted manuscript online: June 20, 2024

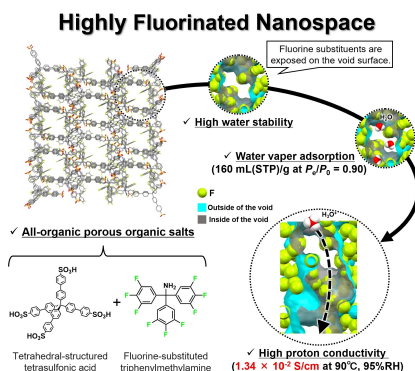
Version of record online: ■■■, ■■■

## Research Article

## Porous Salts

T. Ami, K. Oka,\* S. Kitajima,  
N. Tohnai\* **e202407484**

Highly Fluorinated Nanospace in Porous  
Organic Salts with High Water Stability/  
Capability and Proton Conductivity



This work successfully constructed uniform highly fluorinated nanospaces without impurities such as metals. This highly hydrophobic nanospace exhibits high water stability, and is the first all-organic hydrophobic nanospace where water molecules can enter. Furthermore, this nanospace exhibits very high proton conductivity of  $1.34 \times 10^{-2}$  S/cm at 90 °C and 95 % RH.